Electronic Supplementary Material (ESI) for Dalton Transactions

Supporting Information

A new modification of an old framework: Hofmann layers with unusual tetracyanidometallate groups

Tony D. Keene, Michael J. Murphy, Jason R. Price, David J. Price and Cameron J. Kepert

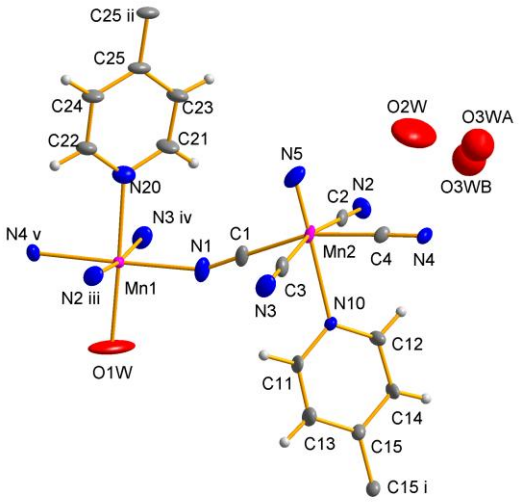

Figure S1 Asymmetric unit and selected symmetry equivalents of **2**. Thermal ellipsoids are at the 50% probability level.

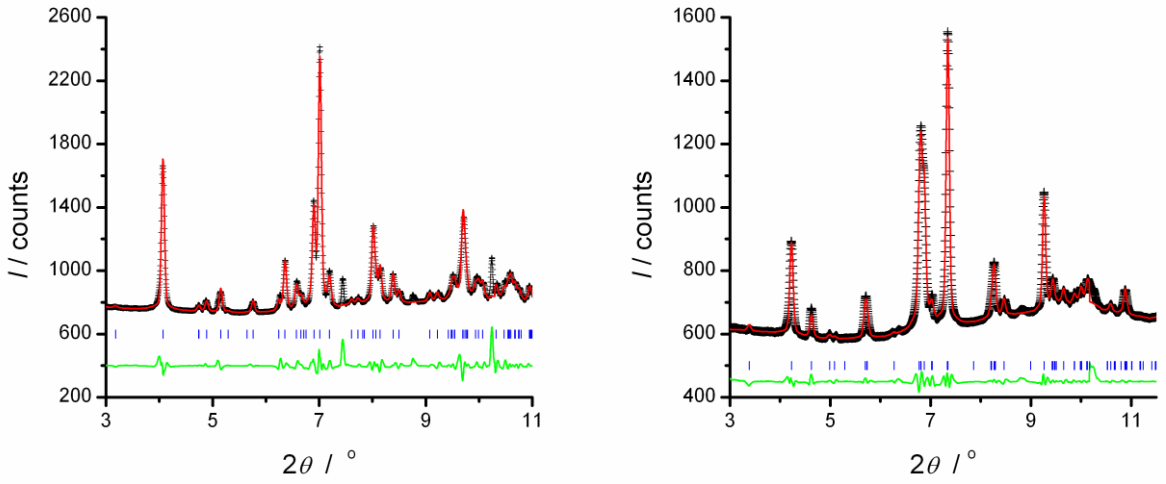

Figure S2 a) Le Bail profile fit to synchrotron PXRD data (λ = 60941 Å) for **1** at 100 K (R_p = 0.978 %, wR_p = 1.537 % and χ^2 = 0.203; a = 7.3775 Å, b = 17.1715 Å, c = 14.3011 Å, β = 91.5856°, V = 1811.0 Å^3) and b) at 500 K (a = 7.5419 Å, b = 16.5071 Å, c = 13.1994 Å, β = 90.100°, V = 1643.3 Å^3).

.

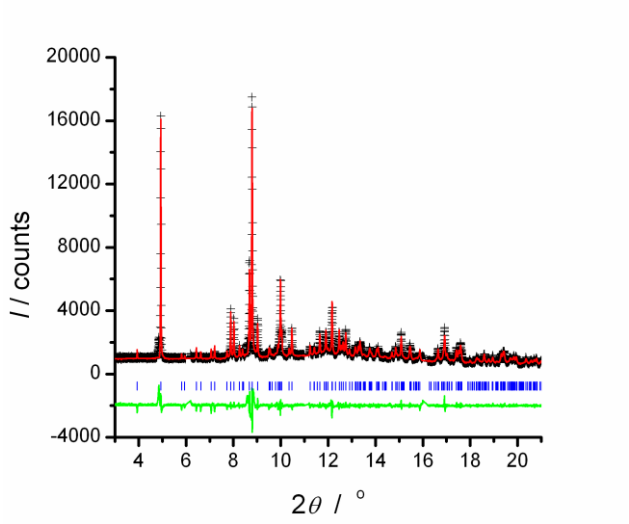

Figure S3 Le Bail profile fit to synchrotron PXRD data (λ = 0.75246 Å) for **2** at 140 K. a = 7.249 Å, b = 17.456 Å, c = 14.029 Å, β = 91.625°, V = 1774.6 Å^3.

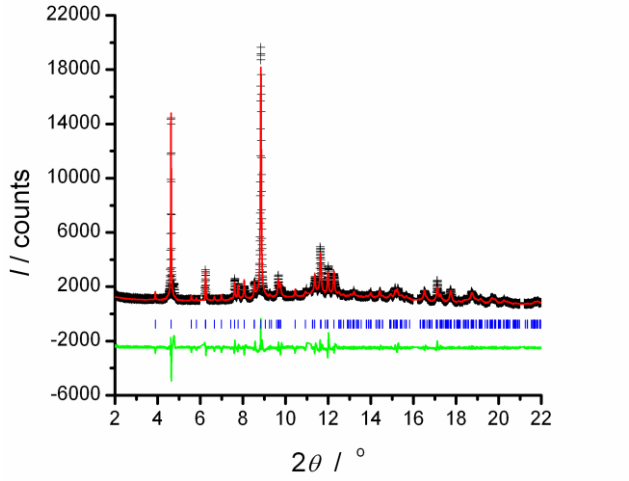

Figure S4 Le Bail profile fit to synchrotron PXRD data (λ = 0.75246 Å) for **3** at 140 K. a = 7.318 Å, b = 17.989 Å, c = 13.860 Å, β = 90.345°, V = 1824.5 Å^3.

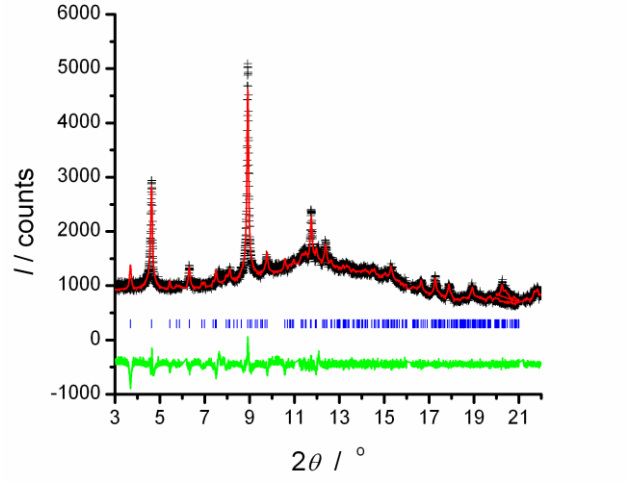

Figure S5 Le Bail profile fit to synchrotron PXRD data (λ = 0.75246 Å) for **4** at 140 K. a = 7.345 Å, b = 18.615 Å, c = 15.028 Å, β = 91.251°, V = 2054.2 Å^3.

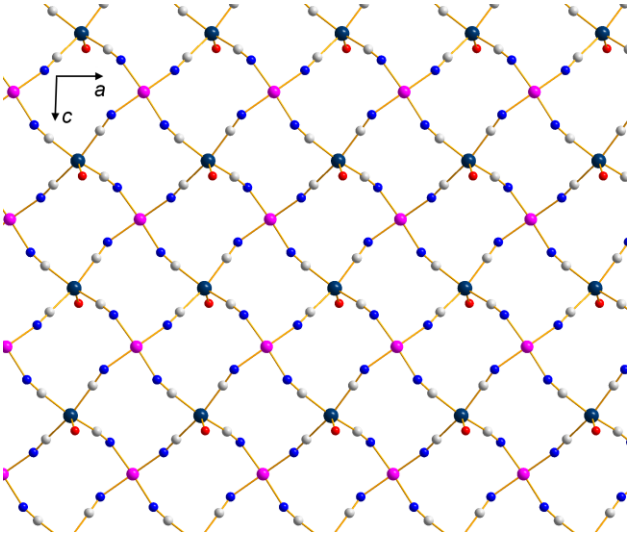

Figure S6 $Mn[MoO(CN)_4]$ Hofmann layer viewed down the *b*-axis in **1**

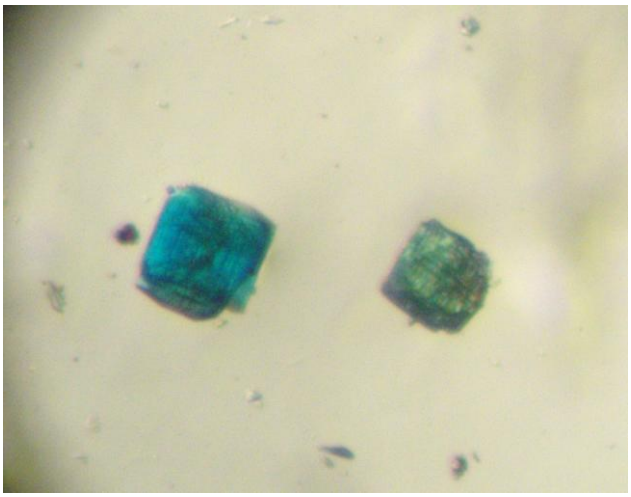

Figure S7 Dichroism of crystals of **5**.

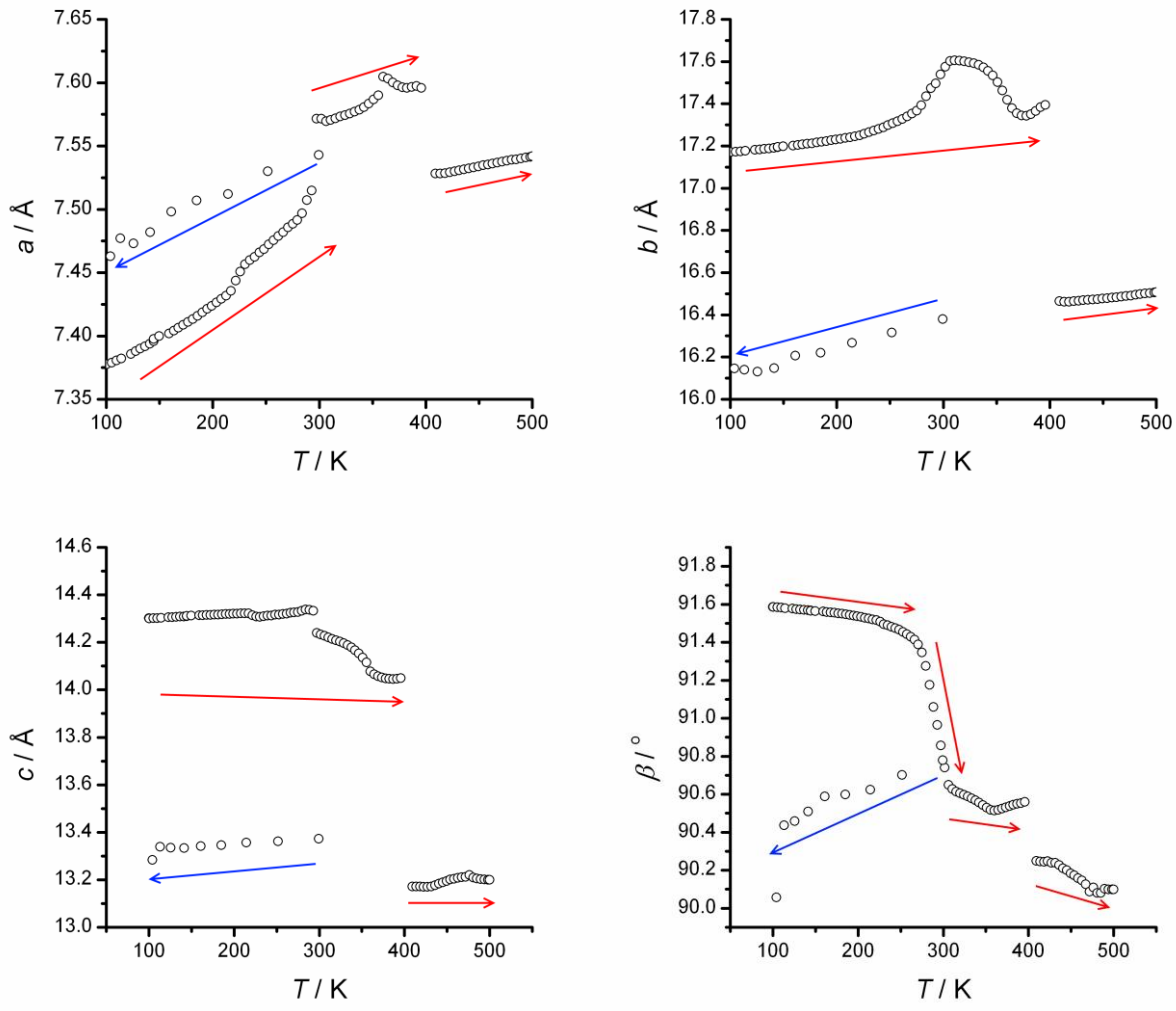

Figure S8 Thermal variation in cell axes and angles in **1**. Red arrows represent heating, blue cooling.

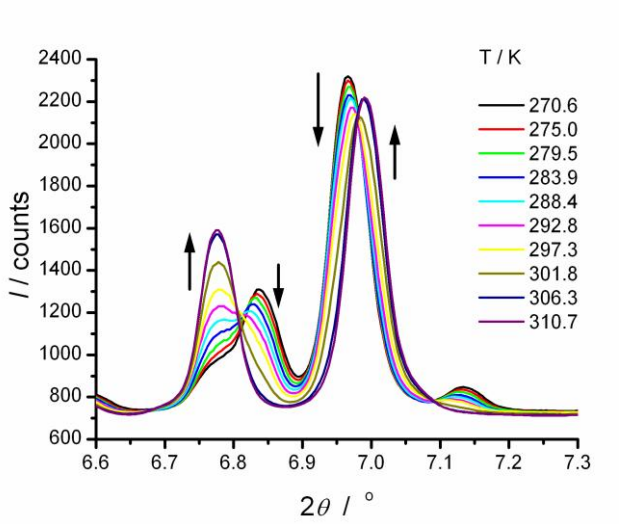

Figure S9 Phase change in **1** between 275 and 306 K. Arrows represent direction of movement with increasing temperature.

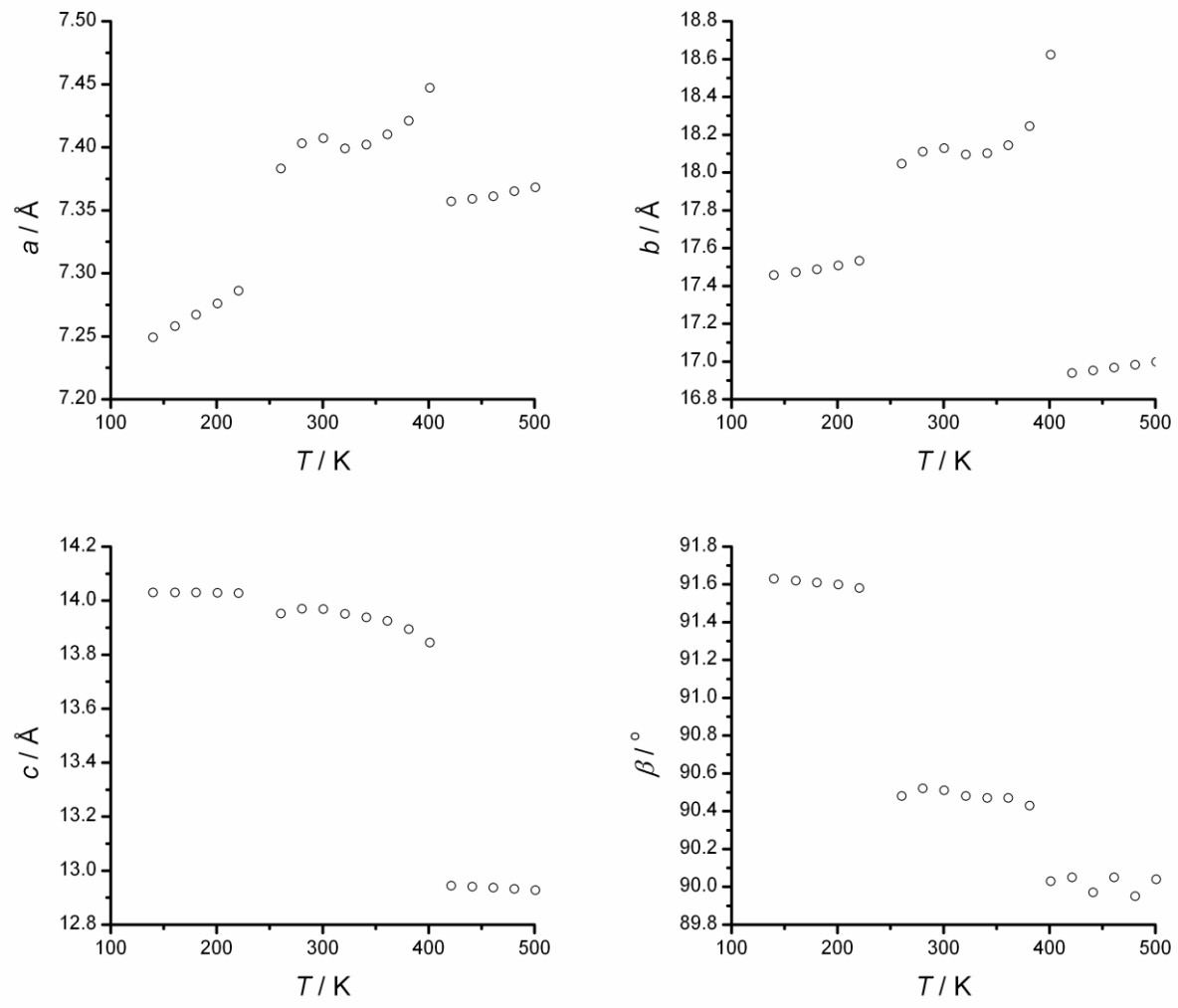

Figure S10 Thermal variation in cell axes and angles in **2**

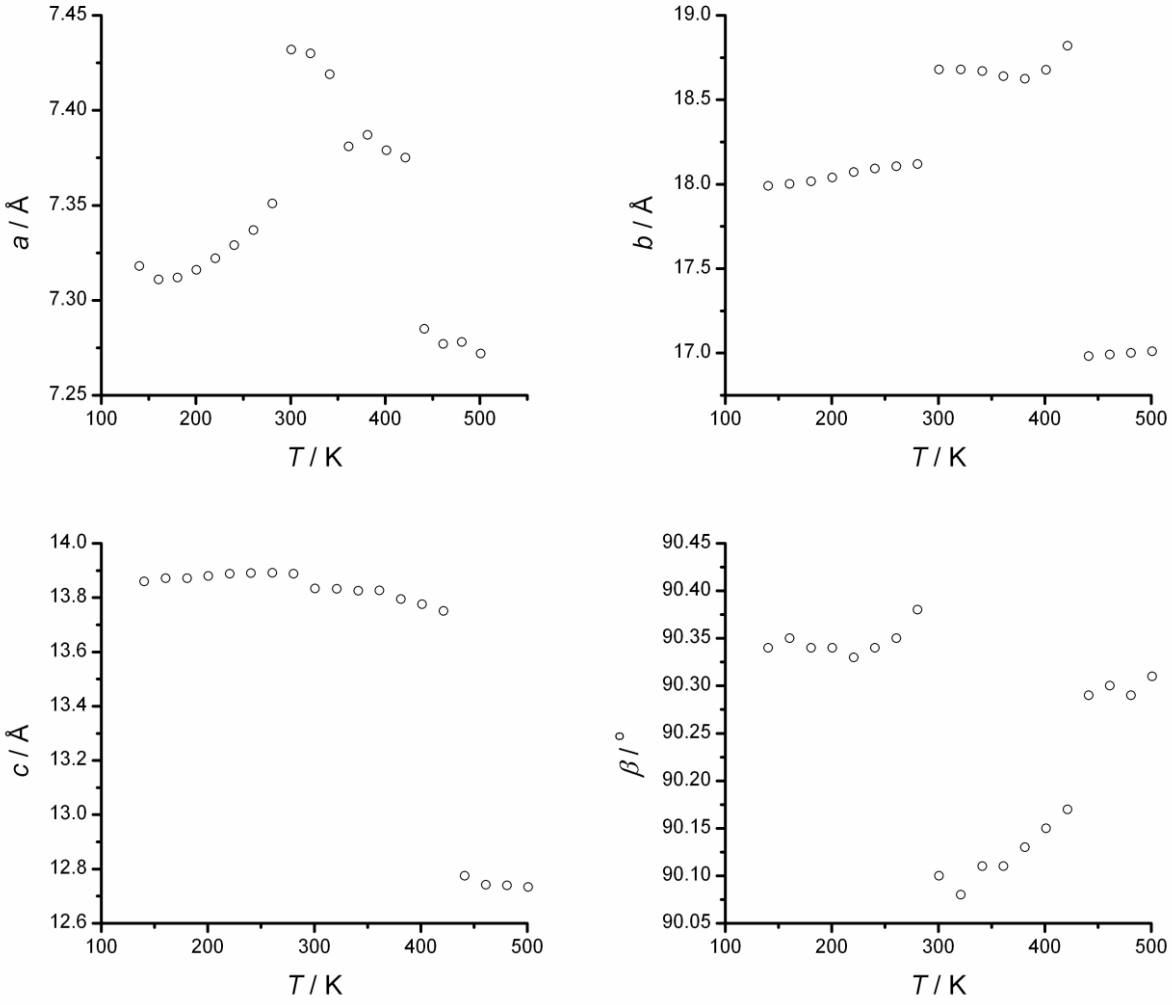

Figure S11 Thermal variation in cell axes and angles in **3**

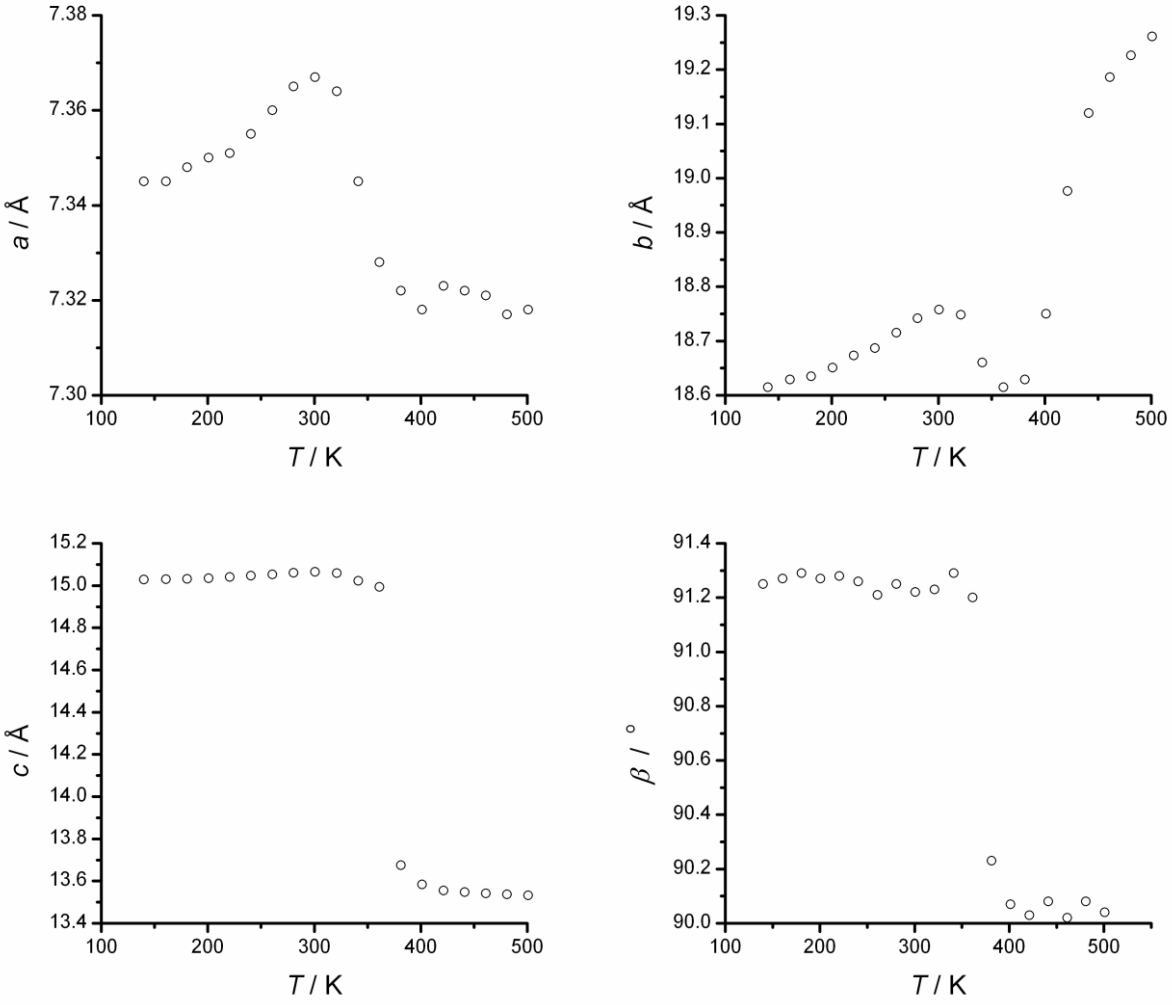

Figure S12 Variation in cell axes and angles in **4**

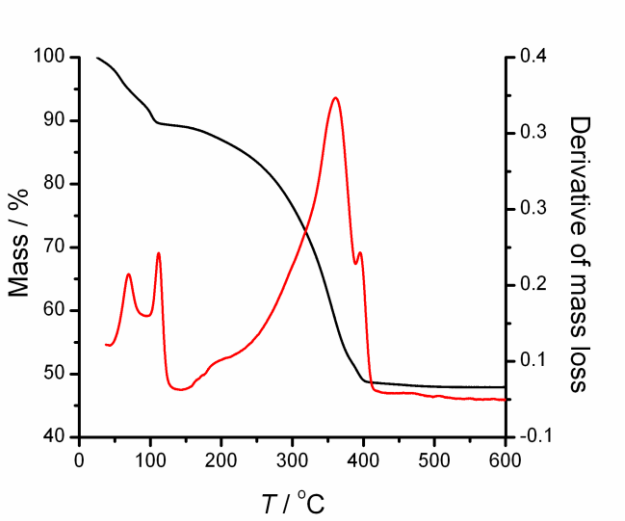

Figure S13 Thermogravimetric analysis plot for **1**. Three mass losses are seen: 22 − 88 °C, centred at 56 °C, corresponding to a loss of two waters (actual 7.2%; calc. 7.5%); 88 – 112 °C , centred at 100 °C, corresponding to the loss of one water (actual 3.2 %; calc. 3.7 %) and a gradual loss from 150 – 400 °C corresponding to the decomposition of the framework into a mixture of MnO_2 and MoO_2 (actual 41.7%; calc. 44.1%).

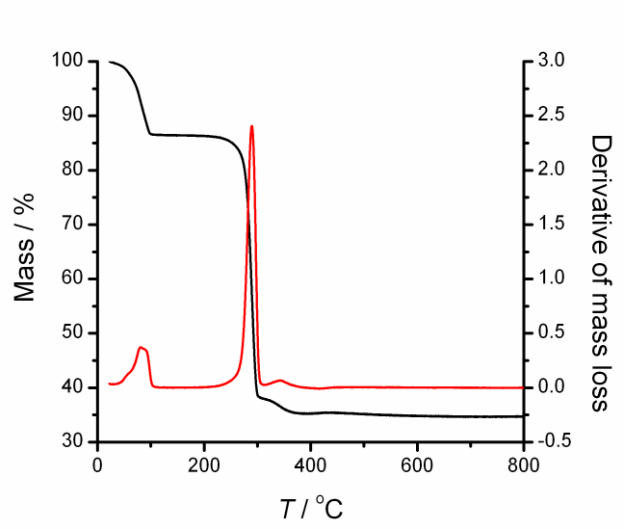

Figure S14 Thermogravimetric analysis plot for **2**. Two mass losses are seen: 45 – 99 °C, centred at 80 °C, corresponding to the loss of three waters (actual 13.5%; calc. 12.3%) and the decomposition of the framework to Mn_2O_3 beginning around 210 °C (actual 51.2%, calc. 51.6%).

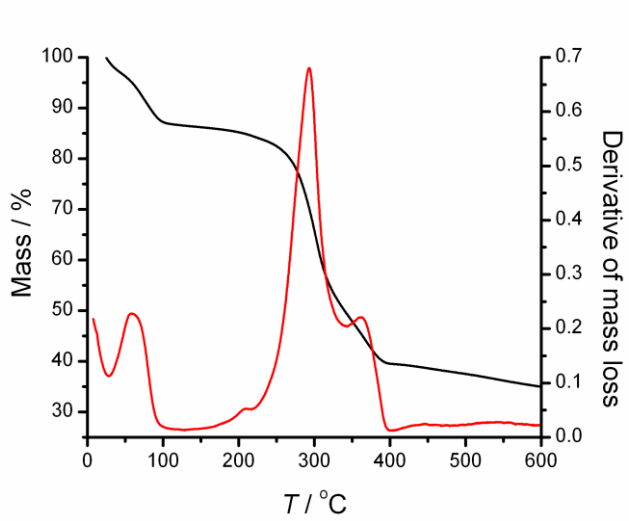

Figure S15 Thermogravimetric analysis plot for **3**. Two mass losses are seen: 22 − 106 °C, centred at 75 °C, corresponding to the loss of three waters (actual 13.1%; calc. 12.3%) and the decomposition of the framework to Fe_2O_3 and Mn_2O_3 beginning around 190 °C (actual 51.5%; calc. 51.8%).

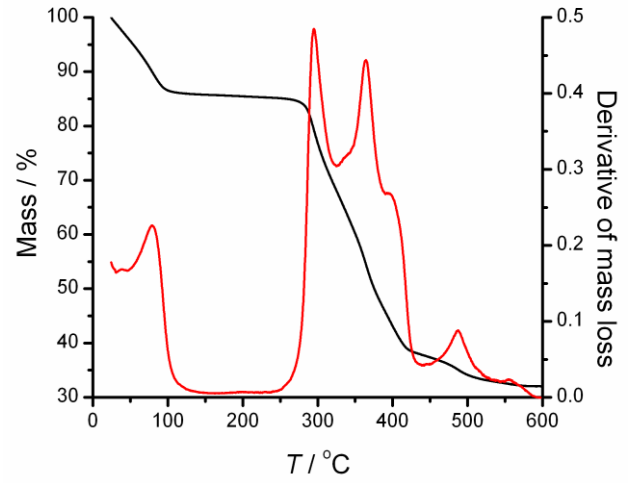

Figure S16 Thermogravimetric analysis plot for **4**. Two mass losses are seen: 22 − 109 °C, centred at 74 °C, corresponding to the loss of three waters (actual 13.1%; calc. 12.3%) and the decomposition of the framework to CoO and Mn_2O_3 beginning above 260 °C (actual 51.2%; calc. 52.9%).

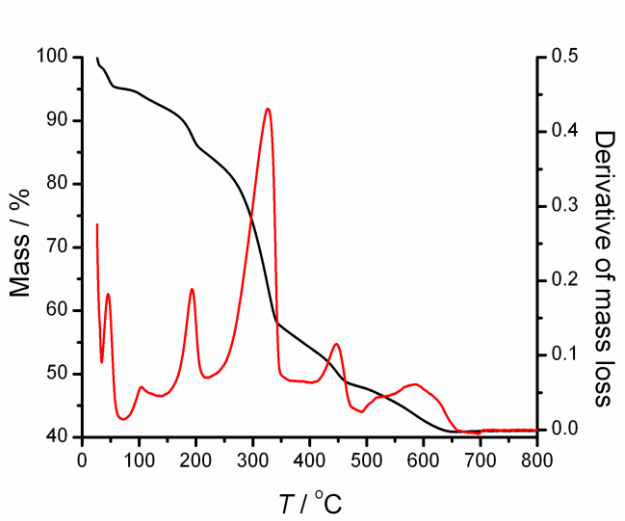

Figure S17 Thermogravimetric analysis plot for **5**. Several mass losses are seen: 22 – 57 °C, corresponding to loss of MeOH, centred at 46 °C (actual 4.9%; calc. 5.6%); 79 – 140 °C corresponding to loss of 2 H_2O, centred at 104 °C (actual 8.4%; calc. 11.8%). After this come four indistinct mass losses, finishing with a total end value of 41.1%. corresponding to the formation of a mixture of Mn_2O_3 and MoO_2.